nature medicine

RIPK3 as a potential therapeutic target for Gaucher's disease

Einat B Vitner[1,4], Ran Salomon[1,4], Tamar Farfel-Becker[1], Anna Meshcheriakova[1], Mohammad Ali[1], Andrés D Klein[1], Frances M Platt[2], Timothy M Cox[3] & Anthony H Futerman[1]

Gaucher's disease (GD), an inherited metabolic disorder caused by mutations in the glucocerebrosidase gene (*GBA*), is the most common lysosomal storage disease[1]. Heterozygous mutations in *GBA* are a major risk factor for Parkinson's disease[2]. GD is divided into three clinical subtypes based on the absence (type 1) or presence (types 2 and 3) of neurological signs. Type 1 GD was the first lysosomal storage disease (LSD) for which enzyme therapy became available, and although infusions of recombinant glucocerebrosidase (GCase) ameliorate the systemic effects of GD, the lack of efficacy for the neurological manifestations, along with the considerable expense[3] and inconvenience of enzyme therapy for patients, renders the search for alternative or complementary therapies paramount. Glucosylceramide and glucosylsphingosine accumulation in the brain leads to massive neuronal loss in patients with neuronopathic GD (nGD)[4] and in nGD mouse models[5–7]. However, the mode of neuronal death is not known. Here, we show that modulating the receptor-interacting protein kinase-3 (Ripk3) pathway markedly improves neurological and systemic disease in a mouse model of GD. Notably, *Ripk3* deficiency substantially improved the clinical course of GD mice, with increased survival and motor coordination and salutary effects on cerebral as well as hepatic injury.

We previously demonstrated elevation of proinflammatory cytokines, including interleukin-1β and tumor necrosis factor-α (Tnf-α)[6], in a mouse model of GD: $Gba^{flox/flox}$; nestin-Cre mice. These mice[7] recapitulate many features of human nGD, although their *Gba* deficiency is restricted to neural and macroglial lineages[5,7]. To determine the mechanism of neuronal cell death, we examined brain pathology in two independent GD models: $Gba^{flox/flox}$; nestin-Cre mice[7] and a chemically induced model in which an irreversible GCase inhibitor, conduritol B epoxide (CBE)[8], was injected intraperitoneally (i.p.) daily into C57BL/6 mice. Although both Nissl[5] and Fluoro-Jade C staining (**Fig. 1a**) detected profound levels of cell death in the cerebral cortex of 16- and 21-d-old $Gba^{flox/flox}$; nestin-Cre mice and 27-d-old CBE-treated mice, we observed no TUNEL-positive cells (**Fig. 1b**). Similarly, there was no elevation in the activity of caspase-9, caspase-3/7 (**Fig. 1c**) (with the exception of a modest elevation in caspase-3/7 at the terminal disease stage in $Gba^{flox/flox}$; nestin-Cre mice) or caspase-8 (**Fig. 1c**) and no cleavage of caspase-8 (**Fig. 1d**) or poly (ADP-ribose) polymerase (Parp1) (**Fig. 1e**), suggesting that neuronal cell death in nGD is caspase independent and nonapoptotic.

Recent work has demonstrated the existence of a form of programmed ne crosis (termed necroptosis) that is dependent on the protein serine-threonine kinases RIPK1 and RIPK3 (ref. 9). Necroptosis can be triggered upon activation of TNF receptors[9] or Toll-like receptors[10], in response to genotoxic stress[11] and during virus infection [12]. Cleavage of these kinases by caspase-8 prevents necroptosis and is associated with apoptosis[13]. However, when caspase-8 is inactive, RIPK1 and RIPK3 are not cleaved but rather engage the effector mechanisms of necroptosis[14]. Recently, the antiapoptotic protein c-FLIP (also known as CFLAR (short for CASP8 and FADD-like apoptosis regulator)), a catalytically inactive homolog of caspase-8, was shown to have an essential role in the regulation of necroptosis[15]. Caspase-8 maintains sufficient proteolytic activity when found in a heterodimer with c-FLIP long (c-$FLIP_L$) to prevent the association of RIPK1, RIPK3 and FADD (Fas-associated protein with death domain)[16], thus inhibiting necroptosis; in contrast, a heterodimer of caspase-8 and c-FLIP short (c-$FLIP_S$) has no proteolytic activity, permitting the assembly of RIPK1 and RIPK3 and thus promoting necroptosis[10]. In both GD mouse models, we detected (by mRNA levels, **Fig. 1f**, and by western blotting, **Fig. 1g**) elevated levels of c-$Flip_S$ in the brains of symptomatic mice, suggesting the presence of a caspase 8–c-$Flip_S$ heterodimer, which would explain the lack of caspase-8 activity (**Fig. 1c**) in the brains of mice with nGD. We detected an elevation in c-$Flip_L$ mRNA levels only at the terminal stage of the disease in $Gba^{flox/flox}$; nestin-Cre mice (**Fig. 1f**).

Increased expression of RIPK1 and RIPK3 and the contribution of these proteins to various pathological conditions such as detachment of the retina[17], macrophage necrosis in atherosclerosis development[18], regulation of virus-induced inflammation[19], systemic inflammatory response syndrome[20] and ethanol-induced liver injury[21] have been reported. All of these pathological states involve necrotic cell death, suggesting that the contribution of RIPK1 and RIPK3 to these pathological states can be attributed to their role in necrosis. To elucidate the role of necroptosis in nGD brains, we analyzed levels of Ripk1 and Ripk3, both of which were markedly elevated (determined by analysis

[1]Department of Biological Chemistry, Weizmann Institute of Science, Rehovot, Israel. [2]Department of Pharmacology, University of Oxford, Oxford, UK. [3]Department of Medicine, University of Cambridge, Cambridge, UK. [4]These authors contributed equally to this work. Correspondence should be addressed to A.H.F. (tony.futerman@weizmann.ac.il).

Received 20 June 2013; accepted 12 December 2013; published online 19 January 2014; doi:10.1038/nm.3449

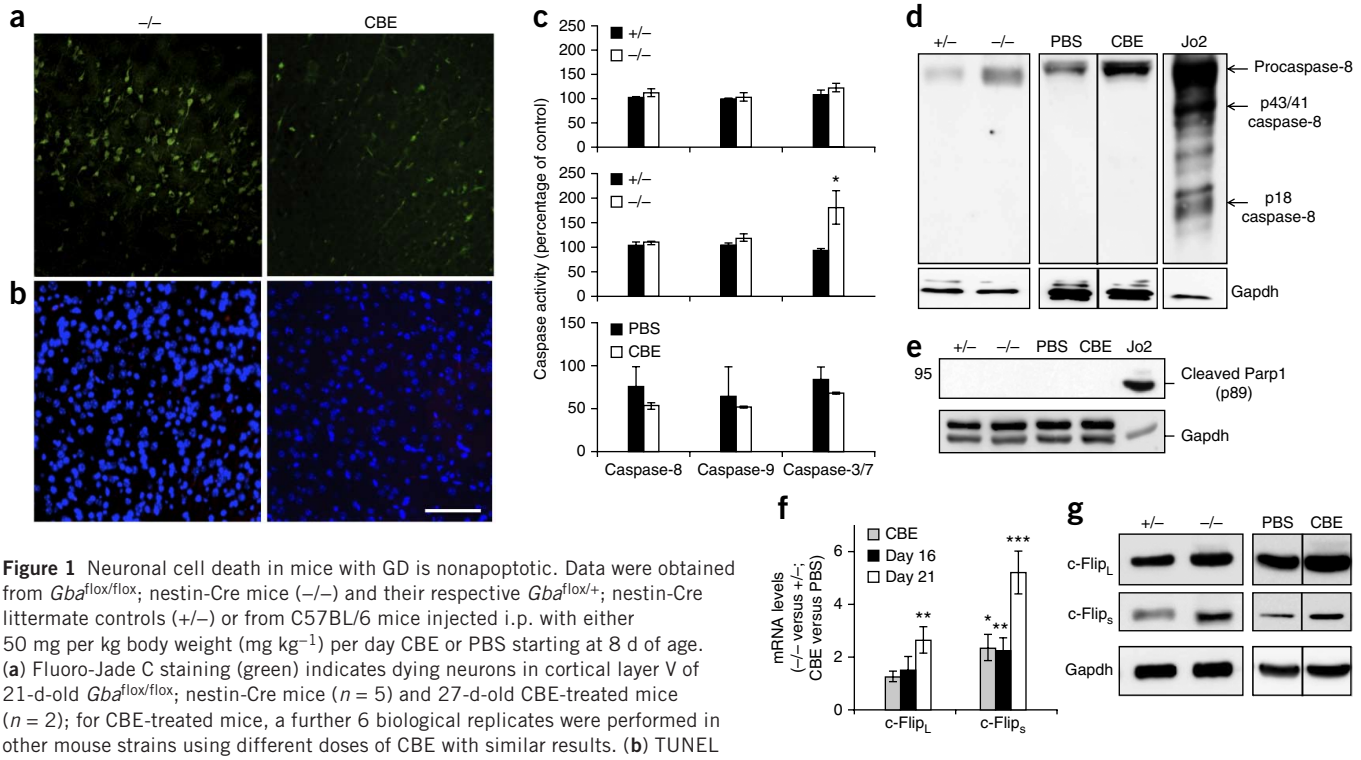

Figure 1 Neuronal cell death in mice with GD is nonapoptotic. Data were obtained from *Gba*$^{flox/flox}$; nestin-Cre mice (–/–) and their respective *Gba*$^{flox/+}$; nestin-Cre littermate controls (+/–) or from C57BL/6 mice injected i.p. with either 50 mg per kg body weight (mg kg^{-1}) per day CBE or PBS starting at 8 d of age. (**a**) Fluoro-Jade C staining (green) indicates dying neurons in cortical layer V of 21-d-old *Gba*$^{flox/flox}$; nestin-Cre mice ($n = 5$) and 27-d-old CBE-treated mice ($n = 2$); for CBE-treated mice, a further 6 biological replicates were performed in other mouse strains using different doses of CBE with similar results. (**b**) TUNEL staining of cortical layer V in 21-d-old *Gba*$^{flox/flox}$; nestin-Cre mice ($n = 3$) and in 27-d-old CBE-treated ($n = 2$) mice. Sections were counterstained with DAPI (blue). No TUNEL staining (red) can be seen. Scale bar for **a** and **b**, 100 µm. (**c**) Activity of caspase-8, caspase-9 and caspase-3/7 in cortical homogenates of 16-d-old (top) and 21-d-old (middle) *Gba*$^{flox/flox}$; nestin-Cre mice and in 27-d-old CBE-treated mice (bottom). Activities were normalized to 100% of the values of control mice. Values are mean ± s.e.m. ($n = 2$ for CBE-treated mice, $n = 7$ for 21-d-old *Gba*$^{flox/flox}$; nestin-Cre mice and $n = 5$ for all others). *$P < 0.05$. (**d**) Western blots of caspase-8 showing full-length caspase-8 (procaspase 8), the cleaved intermediate p43/p41 and the caspase-8 active fragment p18 in homogenates (100 µg protein) from the brains of 27-d-old CBE-treated mice ($n = 2$) and of 21-d-old *Gba*$^{flox/flox}$; nestin-Cre mice ($n = 4$). Gapdh served as a loading control. A liver homogenate from C57BL/6 mice treated with a Fas-activating antibody (Jo2) acted as a control for caspase-8 cleavage. (**e**) Western blots of the cleavage product of Parp1 (M_r of 89 kDa) in homogenates (100 µg protein) from brains of 27-d-old CBE-treated mice ($n = 2$) and 21-d-old *Gba*$^{flox/flox}$; nestin-Cre mice ($n = 4$). Gapdh served as a loading control. A liver homogenate from mice treated with Jo2 acted as a control for Parp1 cleavage. (**f**) RT-PCR of c-Flip$_L$ and c-Flip$_S$ in cortical homogenates from 21-d-old CBE-treated mice ($n = 3$) and 16- and 21-d-old *Gba*$^{flox/flox}$; nestin-Cre mice ($n = 4$). Results are expressed as fold change versus untreated or littermate control mice and are mean ± s.e.m. Cycle threshold (Ct) values were normalized to levels of TATA box–binding protein (Tbp). *$P < 0.05$, **$P < 0.01$, ***$P < 0.001$, between *Gba*$^{flox/flox}$; nestin-Cre versus littermate control mice and between mice treated with CBE versus PBS. (**g**) Western blots of c-Flip$_L$ and c-Flip$_S$ in homogenates (150 µg protein) from brains of 21-d-old *Gba*$^{flox/flox}$; nestin-Cre mice ($n = 4$) and 21-d-old CBE-treated mice ($n = 5$). Gapdh served as a loading control.

of mRNA levels (**Fig. 2a**) and by western blotting (**Fig. 2b**,**c**)) in the brains of symptomatic *Gba*$^{flox/flox}$; nestin-Cre mice. Crucially, levels of RIPK1 were also elevated in the one available brain of a human patient who succumbed to type 2 GD compared to an age-matched control brain (**Supplementary Fig. 1**).

An additional role of RIPK1 and RIPK3 in inflammatory processes has recently been suggested[22]; RIPK1 and RIPK3 may contribute to inflammation independent of cell death by activating the NLRP3 inflammasome[22]. The role of RIPK3 in proinflammatory processes is also supported by the fact that epidermis-specific elimination of caspase-8 leads to chronic inflammation[23,24] that can be suppressed by deletion of *Ripk3* (ref. 25). To elucidate the role of Ripk3, we analyzed whether Ripk3 abundance was increased in microglia, neurons or astrocytes. In brains of *Gba*$^{flox/flox}$; nestin-Cre mice, Ripk3 expression was increased in all Mac-2–positive (i.e., activated) microglia (**Fig. 2d**), consistent with a neuroinflammatory role for Ripk3. Ripk3 was mainly expressed in the nuclei of neurons from *Gba*$^{flox/flox}$; nestin-Cre mice, in contrast to control mice where it was located in the cytoplasm (**Fig. 2e**), which implies a possible role for Ripk3 in neuronal cell death. Translocation of RIPK3 to the nucleus has been observed in HeLa cells upon treatment with leptomycin B[26], but RIPK3 translocation in the central nervous system has not been reported. However, Ripk3 was undetectable in glial fibrillary acidic protein (Gfap)-positive astrocytes, suggesting a lack of involvement of this pathway in activated astrocytes (**Fig. 2d**). A direct correlation was observed between the brain regions that are affected in nGD[5] and the presence of the immunoreactive Ripk3 signal (data not shown). Notably, expression of Ripk1 and Ripk3 were unaltered in brains obtained from mouse models of other LSDs, such as Niemann-Pick type C1, GM1 gangliosidosis and Sandhoff's disease (data not shown). However, Ripk1 and Ripk3 expression was markedly elevated (approximately fivefold and threefold, respectively) in the brains of twitcher mice, which lack β-galactocerebrosidase and are an authentic mouse model of Krabbe's disease[27] (**Fig. 2f**). This indicates that although brain inflammation and microglial activation are shared features of many LSDs[28,29], different pathways of neuroinflammation occur in specific LSDs.

To further explore the role of RIP kinases in GD pathology, we induced GD in *Ripk3*-deficient mice. In contrast to *Ripk1*-null mice, which die 1–3 d after birth[30] and are thus unsuitable for *in vivo*

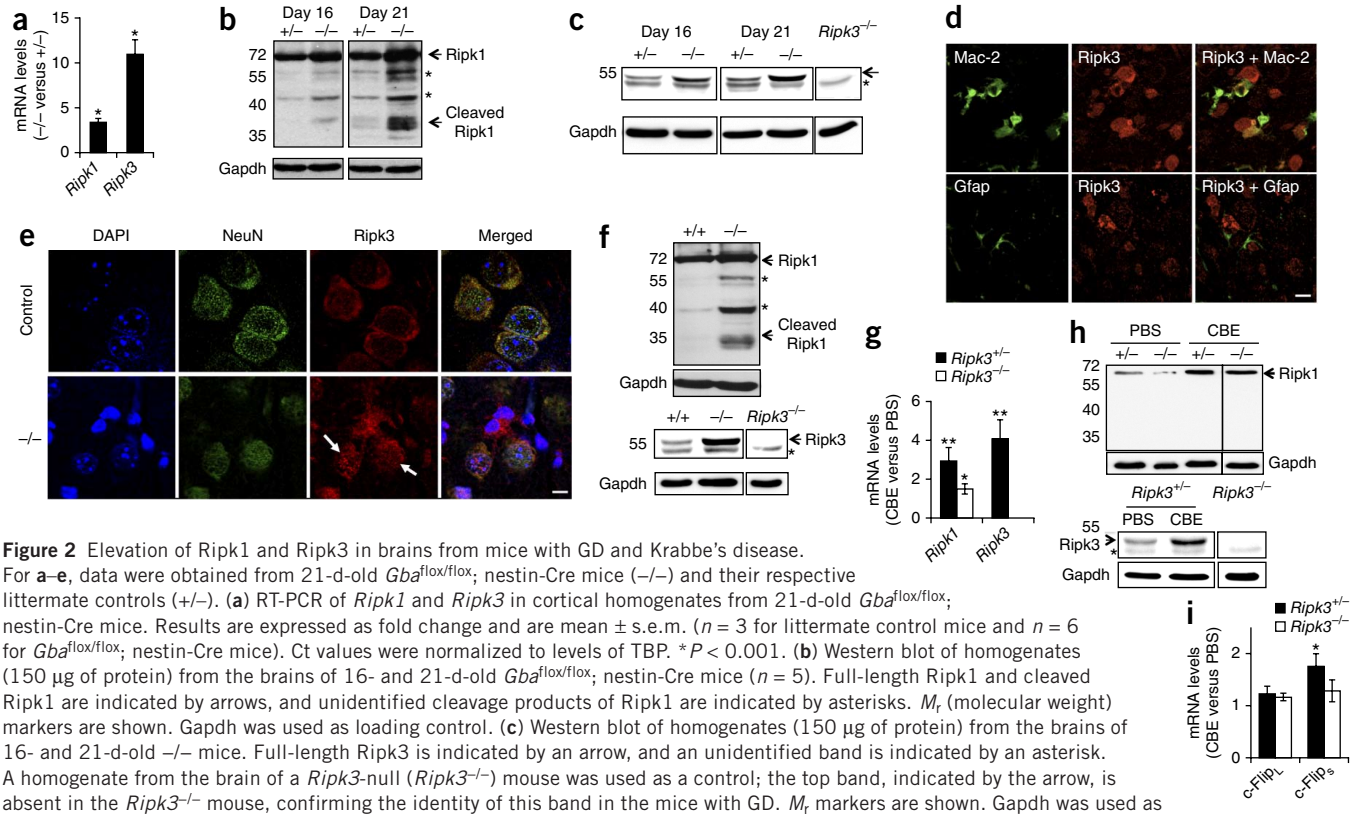

Figure 2 Elevation of Ripk1 and Ripk3 in brains from mice with GD and Krabbe's disease. For **a**–**e**, data were obtained from 21-d-old *Gba*$^{flox/flox}$; nestin-Cre mice (–/–) and their respective littermate controls (+/–). (**a**) RT-PCR of *Ripk1* and *Ripk3* in cortical homogenates from 21-d-old *Gba*$^{flox/flox}$; nestin-Cre mice. Results are expressed as fold change and are mean ± s.e.m. ($n = 3$ for littermate control mice and $n = 6$ for *Gba*$^{flox/flox}$; nestin-Cre mice). Ct values were normalized to levels of TBP. $^{*}P < 0.001$. (**b**) Western blot of homogenates (150 µg of protein) from the brains of 16- and 21-d-old *Gba*$^{flox/flox}$; nestin-Cre mice ($n = 5$). Full-length Ripk1 and cleaved Ripk1 are indicated by arrows, and unidentified cleavage products of Ripk1 are indicated by asterisks. M_r (molecular weight) markers are shown. Gapdh was used as loading control. (**c**) Western blot of homogenates (150 µg of protein) from the brains of 16- and 21-d-old –/– mice. Full-length Ripk3 is indicated by an arrow, and an unidentified band is indicated by an asterisk. A homogenate from the brain of a *Ripk3*-null (*Ripk3*$^{–/–}$) mouse was used as a control; the top band, indicated by the arrow, is absent in the *Ripk3*$^{–/–}$ mouse, confirming the identity of this band in the mice with GD. M_r markers are shown. Gapdh was used as loading control. (**d**) Double immunofluorescence of 16-d-old *Gba*$^{flox/flox}$; nestin-Cre mice using either anti-Ripk3 and anti–Mac-2 (top) or anti-Ripk3 and anti-Gfap (bottom) antibodies. Ripk3 is in red, Mac-2 and Gfap are in green and areas of overlap indicated on the right. Scale bar, 10 µm. Results are representative of three biological replicates. (**e**) Double immunofluorescence of 16-d-old littermate control (control, top) and *Gba*$^{flox/flox}$; nestin-Cre mice (bottom) using DAPI (blue) and anti-NeuN (green) and anti-Ripk3 (red) antibodies; areas of overlap are indicated on the right (merged). Arrows indicate nuclear staining of Ripk3. Scale bar, 10 µm. Results are representative of three biological replicates. (**f**) Western blot of homogenates (150 µg of protein) from the brains of 5-week-old mice with Krabbe's disease (twitcher mice). Blots were probed with anti-Ripk1 or anti-Ripk3 antibodies. Full-length Ripk1, cleaved Ripk1 and Ripk3 bands are indicated by arrows, and unidentified bands on the Ripk1 and Ripk3 blots are indicated by asterisks (*). Results are representative of two biological replicates. A homogenate from the brain of a *Ripk3*$^{–/–}$ mouse was used as a control and Gapdh as a loading control. (**g**) RT-PCR of *Ripk1* and *Ripk3* in cortical homogenates from 28-d-old *Ripk3*$^{+/–}$ (control) and *Ripk3*$^{–/–}$ mice treated with either CBE (25 mg kg$^{–1}$ per day) or PBS from 8 d of age. Results are expressed as fold change and are mean ± s.e.m. ($n = 3$). Ct values were normalized to levels of TBP. $^{*}P < 0.05$, $^{**}P < 0.01$, between *Ripk3*$^{+/–}$ and *Ripk3*$^{–/–}$ mice treated with CBE versus PBS. (**h**) Western blot of homogenates (150 µg of protein) from the brains of 28-d-old *Ripk3*$^{+/–}$ (+/–) and *Ripk3*$^{–/–}$ mice (–/–) treated with either CBE (25 mg kg$^{–1}$ per day) or with PBS from 8 d of age. Top, full-length Ripk1. Bottom, full-length Ripk3 is indicated by an arrow and an unidentified band is indicated by an asterisk. Results are representative of three biological replicates. M_r markers are shown. Gapdh was used as loading control. (**i**) RT-PCR of c-Flip$_L$ and c-Flip$_S$ in cortical homogenates from 28-d-old *Ripk3*$^{+/–}$ (control) and *Ripk3*$^{–/–}$ mice treated with either CBE (25 mg kg$^{–1}$ per day) or with PBS from 8 d of age. Results are expressed as fold change and are mean ± s.e.m. ($n = 3$). Ct values were normalized to levels of TBP. $^{*}P < 0.05$, between *Ripk3*$^{+/–}$ and *Ripk3*$^{–/–}$ mice treated with CBE versus PBS.

studies, *Ripk3*-deficient mice do not show adverse effects in development or in overall health[31]. We induced GD by daily CBE injection[8,32]. We chose the CBE model because GCase activity is inhibited in all cell types and organs upon CBE treatment, in contrast to the *Gba*$^{flox/flox}$; nestin-Cre mouse model in which GCase deficiency is restricted to cells of neuronal lineage. Moreover, the latter model is very severe in disease progression, with mice not surviving beyond 3–4 weeks of age, limiting the available window of therapeutic intervention. Levels of Ripk1 and Ripk3 (determined by analysis of mRNA levels (**Fig. 2g**) and by western blotting (**Fig. 2h**)) and mRNA levels of c-Flip$_S$ (**Fig. 2i**) were markedly elevated in the brains of *Ripk3*$^{+/–}$ CBE-treated mice, which is similar to what is observed in the *Gba*$^{flox/flox}$; nestin-Cre mouse model. Notably, whereas *Ripk3*$^{+/–}$ mice (control mice) injected with CBE displayed typical manifestations of mouse GD[5,8] (i.e., weight loss (**Fig. 3a**) and loss of motor coordination (**Fig. 3b**)), the signs of disease in *Ripk3*$^{–/–}$ mice injected with CBE were considerably ameliorated (**Fig. 3a**,**b**). The lifespan of *Ripk3*$^{–/–}$ mice injected with CBE was significantly extended to >100 d, with survival to 180 d in some animals, whereas no *Ripk3*$^{+/–}$ mice survived beyond 40 d of age (**Fig. 3c**). We observed improvements in motor coordination (**Fig. 3b**) and lifespan (**Fig. 3c**) before appearance of neuronal loss but after appearance of neuroinflammation (**Fig. 3d**) that were accompanied by markedly fewer activated microglia in layer V of the cortex (**Fig. 3d**). These results directly implicate the Ripk3 pathway in neuroinflammation and indicate that this pathway might be a molecular target for therapeutic intervention in nGD.

Moreover, liver injury was also ameliorated in CBE-treated *Ripk3*$^{–/–}$ mice, which showed fewer CD68-positive Kupffer cells (**Fig. 3e**) and a decrease in serum alanine aminotransferase (ALT) activity, suggesting that CBE-induced hepatocyte injury was also attenuated (**Fig. 3f**). Finally, the ratio of spleen weight to body weight, an indicator of GD progression in CBE-treated mice[8], was also improved (**Fig. 3g**). Improvement in the outcome of visceral symptoms, as well as in central nervous system pathology after CBE administration, supports the

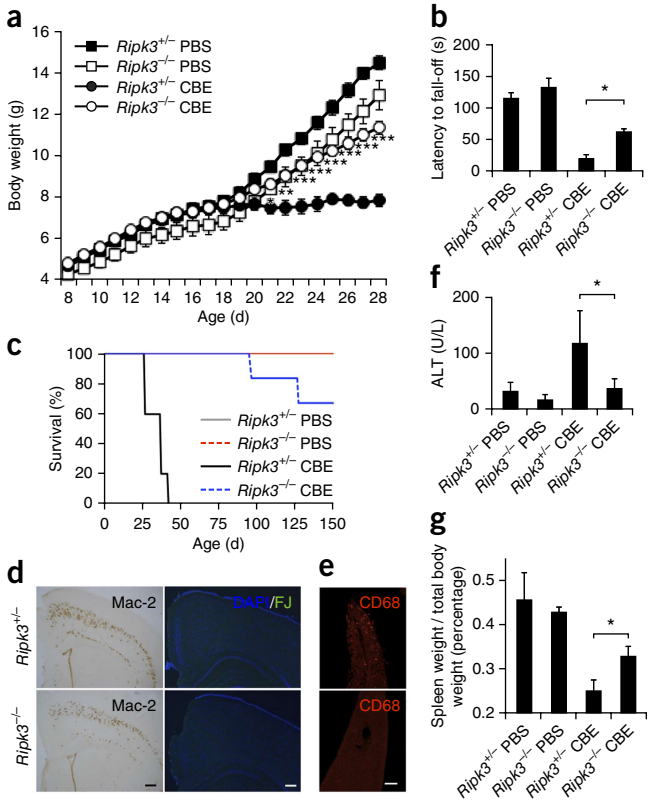

Figure 3 *Ripk3* deficiency improves the clinical course of mice with GD. (**a**) Body weight of *Ripk3*$^{+/-}$ (control, $n = 15$) and *Ripk3*$^{-/-}$ mice ($n = 18$) treated with either CBE or PBS ($n = 9$ for *Ripk3*$^{+/-}$ and $n = 7$ for *Ripk3*$^{-/-}$ mice). Results are mean ± s.e.m. $^{*}P < 0.05$, $^{**}P < 0.01$, $^{***}P < 0.001$, between *Ripk3*$^{+/-}$ and *Ripk3*$^{-/-}$ mice treated with CBE. (**b**) Rotarod performance of 31-d-old *Ripk3*$^{+/-}$ and *Ripk3*$^{-/-}$ mice. $n = 5$ for PBS-treated mice, $n = 6$ for *Ripk3*$^{+/-}$ mice treated with CBE and $n = 10$ for *Ripk3*$^{-/-}$ mice treated with CBE. Results are mean ± s.e.m. $^{*}P < 0.001$. (**c**) Kaplan-Meyer survival curves for *Ripk3*$^{+/-}$ ($n = 5$) and *Ripk3*$^{-/-}$ ($n = 6$) mice. (**d**) Microglial activation (Mac-2) and neuronal loss (Fluoro-Jade C, green) in coronal sections of 28-d-old *Ripk3*$^{+/-}$ and *Ripk3*$^{-/-}$ mice treated with CBE from 8 d of age; DAPI staining is in blue. Results are representative of three biological replicates. Scale bars, 250 µm. No staining was observed in control brains. (**e**) Immunohistochemical staining for the macrophage marker, CD68 (red) in liver sections of 28-d-old *Ripk3*$^{+/-}$ and *Ripk3*$^{-/-}$ mice treated with CBE. Results are representative of three biological replicates. Scale bar, 40 µm. (**f**) Serum ALT in 28-d-old *Ripk3*$^{+/-}$ and *Ripk3*$^{-/-}$ mice treated with CBE or PBS ($n = 3$). Results are mean ± s.d. $^{*}P < 0.05$. (**g**) Spleen weight of 28-d-old *Ripk3*$^{+/-}$ and *Ripk3*$^{-/-}$ mice treated with CBE (25 mg kg^{-1} per day, $n = 5$ for *Ripk3*$^{+/-}$ and $n = 7$ for *Ripk3*$^{-/-}$ mice) or PBS ($n = 3$) for 20 d. Results are mean ± s.e.m. $^{*}P < 0.05$.

hypothesis that Ripk3 is critical for a specific mode of microglia and macrophage activation in the inflammatory response. Notably, we observed no phenotypic difference in the disease induced by CBE in *Tnf*-deficient mice (**Fig. 4a**), and disease progression in these mice was accompanied by elevated Ripk1 (**Fig. 4b**) and Ripk3 (**Fig. 4c**) levels, which suggests that the experimentally induced GD pathology is Ripk3 dependent but Tnf independent.

In conclusion, our results show that Rip kinases are directly involved in the pathway of pathological events in severe forms of GD and also appear to be involved in the acute neuropathological changes in Krabbe's disease. Ripk3 elevation in microglia, together with the improvement in symptoms before neuronal loss and the attenuation of the pathological injury in peripheral organs in *Ripk3*$^{-/-}$ mice with GD, also supports the notion[22,33] that Ripk3 not only is a key activator of necrotic cell death but also orchestrates inflammatory engagement independent of necrosis. The role of Ripk3 in activated microglia and macrophages clearly merits further investigation.

Hitherto, no suitable inhibitors of the Rip kinase pathway displaying *in vivo* activity in brains of mice or humans have been identified. The Ripk1 inhibitor necrostatin-1 has been used to demonstrate the importance of Ripk1 in mediating acute tissue injury[17,34–36], but although necrostatin-1 crosses the blood-brain barrier, it has a half-life of ~1h, which means it is unsuitable for treatment of chronic diseases such as GD[37,38]. A Ripk3 inhibitor[39] and an inhibitor of necrosis downstream to RIPK3 (ref. 40) have demonstrable effects on mouse and human cell lines, but have not been shown, to date, to display efficacy *in vivo* or to cross the blood-brain barrier. Development of such inhibitors may pave the way for alternative therapeutic approaches for all three subtypes of GD and potentially also for Krabbe's disease, for which innovative treatment is urgently required.

METHODS

Methods and any associated references are available in the online version of the paper.

Note: Any Supplementary Information and Source Data files are available in the online version of the paper.

ACKNOWLEDGMENTS

We thank B. Cachón-González (University of Cambridge) for providing twitcher mouse tissue, D. Wallach (Weizmann Institute of Science, Israel) for providing *Tnf* and *Ripk3* knockout mice, R. Schiffmann (Baylor Research Institute) for postmortem human brain tissue, V. Kiss (Weizmann Institute of Science) for help with fluorescence microscopy and N. Platt (University of Oxford) for helpful comments. This work was supported by the Children's Gaucher Research Fund. A.H.F. is the incumbent of an endowed professorial chair supported by the Joseph Meyerhoff family. F.M.P. is a Royal Society Wolfson Research Merit Award holder.

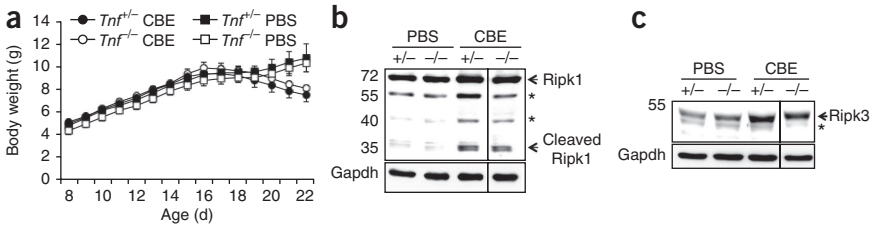

Figure 4 The clinical course of mice with GD is Tnf independent. (**a**) Body weight of *Tnf*$^{+/-}$ (control, $n = 4$) and *Tnf*$^{-/-}$ ($n = 3$) mice treated with either CBE (50 mg kg^{-1} per day) or PBS ($n = 3$ for *Tnf*$^{+/-}$ and $n = 4$ for *Tnf*$^{-/-}$ mice) from 8 d of age. Results are mean ± s.e.m. (**b**,**c**) Western blot of homogenates (150 µg of protein) from the brains of 22-d-old *Tnf*$^{+/-}$ (+/–) and *Tnf*$^{-/-}$ (–/–) mice treated with either CBE (50 mg kg^{-1} per day) or PBS from 8 d of age. Full-length Ripk1 and cleaved Ripk1 are indicated by arrows, and unidentified cleavage products of Ripk1 are indicated by asterisks (**b**). Full-length Ripk3 is indicated by an arrow, and an unidentified band is indicated by an asterisk (**c**). Results are representative of three biological replicates. M_r markers are shown. Gapdh was used as loading control.

AUTHOR CONTRIBUTIONS
E.B.V. and R.S. planned and performed most of the experiments and wrote the manuscript. T.F.-B., A.M., M.A. and A.D.K. performed specific experiments, and F.M.P. and T.M.C. participated in experimental design and provided tissues. A.H.F. participated in experimental design, supervised and funded the project and wrote the manuscript.

COMPETING FINANCIAL INTERESTS
The authors declare no competing financial interests.

Reprints and permissions information is available online at http://www.nature.com/reprints/index.html.

1. Futerman, A.H. & van Meer, G. The cell biology of lysosomal storage disorders. *Nat. Rev. Mol. Cell Biol.* **5**, 554–565 (2004).
2. Eblan, M.J., Walker, J.M. & Sidransky, E. The glucocerebrosidase gene and Parkinson's disease in Ashkenazi Jews. *N. Engl. J. Med.* **352**, 728–731 (2005).
3. Cox, T.M. Competing for the treasure in exceptions. *Am. J. Hematol.* **88**, 163–165 (2013).
4. Wong, K. *et al.* Neuropathology provides clues to the pathophysiology of Gaucher disease. *Mol. Genet. Metab.* **82**, 192–207 (2004).
5. Farfel-Becker, T. *et al.* Spatial and temporal correlation between neuron loss and neuroinflammation in a mouse model of neuronopathic Gaucher disease. *Hum. Mol. Genet.* **20**, 1375–1386 (2011).
6. Vitner, E.B., Farfel-Becker, T., Eilam, R., Biton, I. & Futerman, A.H. Contribution of brain inflammation to neuronal cell death in neuronopathic forms of Gaucher's disease. *Brain* **135**, 1724–1735 (2012).
7. Enquist, I.B. *et al.* Murine models of acute neuronopathic Gaucher disease. *Proc. Natl. Acad. Sci. USA* **104**, 17483–17488 (2007).
8. Kanfer, J.N., Legler, G., Sullivan, J., Raghavan, S.S. & Mumford, R.A. The Gaucher mouse. *Biochem. Biophys. Res. Commun.* **67**, 85–90 (1975).
9. Vandenabeele, P., Galluzzi, L., Vanden Berghe, T. & Kroemer, G. Molecular mechanisms of necroptosis: an ordered cellular explosion. *Nat. Rev. Mol. Cell Biol.* **11**, 700–714 (2010).
10. Feoktistova, M. *et al.* cIAPs block Ripoptosome formation, a RIP1/caspase-8 containing intracellular cell death complex differentially regulated by cFLIP isoforms. *Mol. Cell* **43**, 449–463 (2011).
11. Tenev, T. *et al.* The Ripoptosome, a signaling platform that assembles in response to genotoxic stress and loss of IAPs. *Mol. Cell* **43**, 432–448 (2011).
12. Upton, J.W., Kaiser, W.J. & Mocarski, E.S. Virus inhibition of RIP3-dependent necrosis. *Cell Host Microbe* **7**, 302–313 (2010).
13. Lin, Y., Devin, A., Rodriguez, Y. & Liu, Z.G. Cleavage of the death domain kinase RIP by caspase-8 prompts TNF-induced apoptosis. *Genes Dev.* **13**, 2514–2526 (1999).
14. Zhang, D.-W. *et al.* RIP3, an energy metabolism regulator that switches TNF-induced cell death from apoptosis to necrosis. *Science* **325**, 332–336 (2009).
15. Silke, J. & Strasser, A. The FLIP side of life. *Sci. Signal.* **6**, pe2 (2013).
16. Oberst, A. *et al.* Catalytic activity of the caspase-8-FLIP(L) complex inhibits RIPK3-dependent necrosis. *Nature* **471**, 363–367 (2011).
17. Trichonas, G. *et al.* Receptor interacting protein kinases mediate retinal detachment-induced photoreceptor necrosis and compensate for inhibition of apoptosis. *Proc. Natl. Acad. Sci. USA* **107**, 21695–21700 (2010).
18. Lin, J. *et al.* A role of RIP3-mediated macrophage necrosis in atherosclerosis development. *Cell Rep.* **3**, 200–210 (2013).
19. Cho, Y.S. *et al.* Phosphorylation-driven assembly of the RIP1–RIP3 complex regulates programmed necrosis and virus-induced inflammation. *Cell* **137**, 1112–1123 (2009).
20. Duprez, L. *et al.* RIP kinase–dependent necrosis drives lethal systemic inflammatory response syndrome. *Immunity* **35**, 908–918 (2011).
21. Roychowdhury, S., McMullen, M.R., Pisano, S.G., Liu, X. & Nagy, L.E. Absence of receptor interacting protein kinase 3 prevents ethanol-induced liver injury. *Hepatology* **57**, 1773–1783 (2013).
22. Kang, T.-B., Yang, S.-H., Toth, B., Kovalenko, A. & Wallach, D. Caspase-8 blocks kinase RIPK3-mediated activation of the NLRP3 inflammasome. *Immunity* **38**, 27–40 (2013).
23. Kovalenko, A. *et al.* Caspase-8 deficiency in epidermal keratinocytes triggers an inflammatory skin disease. *J. Exp. Med.* **206**, 2161–2177 (2009).
24. Lee, P. *et al.* Dynamic expression of epidermal caspase 8 simulates a wound healing response. *Nature* **458**, 519–523 (2009).
25. Kaiser, W.J. *et al.* RIP3 mediates the embryonic lethality of caspase-8–deficient mice. *Nature* **471**, 368–372 (2011).
26. Yang, Y., Ma, J., Chen, Y. & Wu, M. Nucleocytoplasmic shuttling of receptor-interacting protein 3 (RIP3): identification of novel nuclear export and import signals in RIP3. *J. Biol. Chem.* **279**, 38820–38829 (2004).
27. Suzuki, K. & Taniike, M. Murine model of genetic demyelinating disease: the twitcher mouse. *Microsc. Res. Tech.* **32**, 204–214 (1995).
28. Vitner, E.B., Platt, F.M. & Futerman, A.H. Common and uncommon pathogenic cascades in lysosomal storage diseases. *J. Biol. Chem.* **285**, 20423–20427 (2010).
29. Vitner, E.B. *et al.* Altered expression and distribution of cathepsins in neuronopathic forms of Gaucher disease and in other sphingolipidoses. *Hum. Mol. Genet.* **19**, 3583–3590 (2010).
30. Kelliher, M.A. *et al.* The death domain kinase RIP mediates the TNF-induced NF-κB signal. *Immunity* **8**, 297–303 (1998).
31. Newton, K., Sun, X. & Dixit, V.M. Kinase RIP3 is dispensable for normal NF-κ Bs, signaling by the B-cell and T-cell receptors, tumor necrosis factor receptor 1, and Toll-like receptors 2 and 4. *Mol. Cell. Biol.* **24**, 1464–1469 (2004).
32. Farfel-Becker, T., Vitner, E.B. & Futerman, A.H. Animal models for Gaucher disease research. *Dis. Model. Mech.* **4**, 746–752 (2011).
33. Wallach, D., Kovalenko, A. & Kang, T.-B. 'Necrosome'-induced inflammation: must cells die for it? *Trends Immunol.* **32**, 505–509 (2011).
34. Chavez-Valdez, R., Martin, L.J., Flock, D.L. & Northington, F.J. Necrostatin-1 attenuates mitochondrial dysfunction in neurons and astrocytes following neonatal hypoxia-ischemia. *Neuroscience* **219**, 192–203 (2012).
35. Rosenbaum, D.M. *et al.* Necroptosis, a novel form of caspase-independent cell death, contributes to neuronal damage in a retinal ischemia-reperfusion injury model. *J. Neurosci. Res.* **88**, 1569–1576 (2010).
36. You, Z. *et al.* Necrostatin-1 reduces histopathology and improves functional outcome after controlled cortical impact in mice. *J. Cereb. Blood Flow Metab.* **28**, 1564–1573 (2008).
37. Jagtap, P.G. *et al.* Structure-activity relationship study of tricyclic necroptosis inhibitors. *J. Med. Chem.* **50**, 1886–1895 (2007).
38. Zhu, S., Zhang, Y., Bai, G. & Li, H. Necrostatin-1 ameliorates symptoms in R6/2 transgenic mouse model of Huntington's disease. *Cell Death Dis.* **2**, e115 (2011).
39. Kaiser, W.J. *et al.* Toll-like receptor 3–mediated necrosis via TRIF, RIP3 and MLKL. *J. Biol. Chem.* **288**, 31268–31279 (2013).
40. Sun, L. *et al.* Mixed lineage kinase domain-like protein mediates necrosis signaling downstream of RIP3 kinase. *Cell* **148**, 213–227 (2012).

ONLINE METHODS

Animals and brain tissues. *Gba*$^{flox/flox}$ mice were crossed with *Gba*$^{flox/+}$; nestin-Cre mice to generate *Gba*$^{flox/flox}$; nestin-Cre mice[7] and *Gba*$^{flox/+}$; nestin-Cre mice, which served as healthy controls. Genotyping was performed by PCR using genomic DNA extracted from mouse tails or embryonic brains[41]. Both male and female mice were used. The colony was maintained in the experimental animal center of the Weizmann Institute of Science. All animal experiments were approved by the Weizmann Institute Institutional Animal Care and Use Committee. Mice deficient in galactocerebrosidase (twitcher mice) were used as a model of Krabbe's disease[27], and mice deficient in the β subunit of β-hexosaminidase A and B were used as a model of Sandhoff's disease[42]. Brains from a mouse model of the GM1 gangliosidosis[43], defective in lysosomal β-galactosidase, and from Niemann-Pick disease type C1 (ref. 44) mice, defective in the *Npc1* gene, were also used. Mice deficient in Tnf (strain B6; 129S6–Tnftm1Gkl/J, The Jackson Laboratory) were provided by D. Wallach. C57BL/6 mice (The Jackson Laboratory) were injected daily i.p. with 50 mg CBE per kg body weight per day[8] or with PBS from 8 d of age. *Ripk3*$^{-/-}$ mice[31] were provided by Genentech (South San Francisco, CA) and backcrossed with C57BL/6 mice to generate *Ripk3*$^{+/-}$ mice. *Ripk3*$^{+/-}$ mice were crossed with *Ripk3*$^{-/-}$ mice to generate *Ripk3*$^{+/-}$ and *Ripk3*$^{-/-}$ littermates. *Ripk3*$^{+/-}$ and *Ripk3*$^{-/-}$ mice were injected daily i.p. with 25 mg CBE per kg body weight per day[8] or with PBS from 8 d of age. No animals were excluded from the study, the sample size was chosen so as to validate statistical analyses, no randomization was used and the investigator was not blinded.

Human brain tissue. A control human brain from an infant who died at birth was provided by the University of Miami Brain and Tissue Bank for Developmental Disorders. The control brain was frozen within 6–26 h of death. A brain sample from a type 2 GD patient, who died at 1 year of age, was obtained with informed consent.

Histochemistry. Tissue was prepared as described[29]. Paraffin sections were incubated with an antibody to Ripk3 (ref. 45) (1:100, ProSci, 2283), an antibody to NeuN[6] (1:50, Chemicon, MAB377), an antibody to Mac-2 (ref. 5) (1:250, Cedarlane, CL8942AP) and an antibody to Gfap[5] (1:100, Dako, Z0334). Counterstaining was performed with DAPI (Molecular Probes, Eugene, OR, USA) (1:2,000, 1 min). Apoptotic cells were detected using TUNEL (ApopTag Red *in situ* kit, Chemicon, Temecula, CA). Kupffer cells were stained with a rat antibody to CD68 (ref. 46) (1:1,000, Serotec, MCA1957) on floating sections. Degenerating neurons were stained with the anionic fluorescein derivative, Fluoro-Jade C, according to manufacturer's instructions (HistoChem, Jefferson, AR).

Caspase activity. Caspase-3/7 (caspase 3 and 7 share the same substrate), caspase-8 and caspase-9 were assayed using a Caspase-Glo assay kit (Promega).

RNA extraction and quantitative PCR. Cortical tissues were used for total RNA extraction. Total RNA isolation, cDNA synthesis and quantitative RT-PCR were performed as described[29]. The relative amounts of mRNA were calculated from the cycle threshold (Ct) values using TBP for normalization. Quantitative PCR was performed using the SYBR Green method with the following primers: TBP forward 5′-TGCTGTTGGTGATTGTTGGT-3′ and TBP reverse 5′-CTGGCTTGTGTGGGAAAGAT-3′; Ripk1 forward 5′-AGTCGAGACTGAAGGACACAGCACT-3′ and Ripk1 reverse 5′-TCCAGCAGGTCACTGGATGCCAT-3′; Ripk3 forward 5′-CTTGAACCCTCCGCTCCTGC-3′ and Ripk3 reverse 5′-AATCTGCTAGCTT GGCGTGG-3′; c-Flip$_L$ forward 5′-ACATGTGTGCTCTGTGGAGG-3′ and c-Flip$_L$ reverse 5′-TGCCTGGCTGATTCTGTCTC-3′; and c-Flip$_S$ forward 5′-ACCTCACGGAACTCATGTCC-3′ and c-Flip$_S$ reverse 5′-TGGGTAGATTCTCTGTGCATGG-3′. *P* values were calculated using a one-tailed two–independent sample Student's *t*-test. A *P* value ≤0.05 was considered statistically significant.

Protein extraction and western blotting. Homogenates were prepared as described[29]. Blots were incubated with the following antibodies: rabbit antibody to RIP1 (ref. 47) (1:1,000, Cell signaling, 3493), rabbit antibody to cleaved PARP[48] (1:1,000, Cell Signaling, 9544), rabbit antibody to RIPK3 (ref. 45) (1:1,000, ProSci, 2283), rat antibody to caspase-8 (ref. 23) (1:2,000, Enzo Biochem, ALX–804–448), rabbit antibody to FLIP[49] (1:1,000, Cell Signaling, 3210) and a mouse antibody to GAPDH[6] (1:10,000, Chemicon, MAB374), followed by incubation with a horseradish peroxidase–conjugated secondary antibody (anti-rabbit 111-035-003, anti-rat 112-035-003 and anti-mouse 115-035-003, 1:10,000, Jackson ImmunoResearch). Bound antibodies were detected using the SuperSignal West Pico chemiluminescent substrate (Thermo Scientific).

Serum alanine aminotransferase. ALT was detected using Spotchem II strips (Arkray, Japan).

Behavioral testing. A rotarod test (Harvard equipment) was used to evaluate rotarod behavior in 31-d-old mice using an accelerating paradigm (4 min on the rotarod at 40 r.p.m.).

Statistical analyses. All data are shown as mean ± s.e.m. Comparisons between two samples were performed using a two-tailed Student's *t*-test. $P < 0.05$ was considered statistically significant.

41. Farfel-Becker, T. *et al.* No evidence for activation of the unfolded protein response in neuronopathic models of Gaucher disease. *Hum. Mol. Genet.* **18**, 1482–1488 (2009).
42. Sango, K. *et al.* Mouse models of Tay-Sachs and Sandhoff diseases differ in neurologic phenotype and ganglioside metabolism. *Nat. Genet.* **11**, 170–176 (1995).
43. Hahn, C.N. *et al.* Generalized CNS disease and massive GM1-ganglioside accumulation in mice defective in lysosomal acid β-galactosidase. *Hum. Mol. Genet.* **6**, 205–211 (1997).
44. Pentchev, P.G. *et al.* A genetic storage disorder in BALB/C mice with a metabolic block in esterification of exogenous cholesterol. *J. Biol. Chem.* **259**, 5784–5791 (1984).
45. Narayan, N. *et al.* The NAD-dependent deacetylase SIRT2 is required for programmed necrosis. *Nature* **492**, 199–204 (2012).
46. Lopez, M.E., Klein, A.D., Dimbil, U.J. & Scott, M.P. Anatomically defined neuron-based rescue of neurodegenerative Niemann-Pick type C disorder. *J. Neurosci.* **31**, 4367–4378 (2011).
47. van Raam, B.J., Ehrnhoefer, D.E., Hayden, M.R. & Salvesen, G.S. Intrinsic cleavage of receptor-interacting protein kinase-1 by caspase-6. *Cell Death Differ.* **20**, 86–96 (2013).
48. Hung, T. *et al.* Extensive and coordinated transcription of noncoding RNAs within cell-cycle promoters. *Nat. Genet.* **43**, 621–629 (2011).
49. Han, J., Sridevi, P., Ramirez, M., Ludwig, K.J. & Wang, J.Y.J. β-Catenin-dependent lysosomal targeting of internalized tumor necrosis factor-α suppresses caspase-8 activation in apoptosis-resistant colon cancer cells. *Mol. Biol. Cell* **24**, 465–473 (2013).

doi:10.1038/nm.3449